Structure, Vol. 11, 295–307, March, 2003, ©2003 Elsevier Science Ltd. All rights reserved. PII S0969-2126(03)00031-5

Dissecting the Assembly of $A\beta_{16-22}$ Amyloid Peptides into Antiparallel β Sheets

Dmitri K. Klimov* and D. Thirumalai*
Institute for Physical Science and Technology
University of Maryland
College Park, Maryland 20742

Summary

Multiple long molecular dynamics simulations are used to probe the oligomerization mechanism of $A\beta_{16-22}$ (KLVFFAE) peptides. The peptides, in the monomeric form, adopt either compact random-coil or extended β strand-like structures. The assembly of the low-energy oligomers, in which the peptides form antiparallel β sheets, occurs by multiple pathways with the formation of an obligatory α-helical intermediate. This observation and the experimental results on fibrillogenesis of $A\beta_{1-40}$ and $A\beta_{1-42}$ peptides suggest that the assembly mechanism (random coil → α helix → β strand) is universal for this class of peptides. In $A\beta_{16-22}$ oligomers both interpeptide hydrophobic and electrostatic interactions are critical in the formation of the antiparallel β sheet structure. Mutations of either hydrophobic or charged residues destabilize the oligomer, which implies that the 16-22 fragments of Arctic (E22G), Dutch (E22Q), and Italian (E22K) mutants are unlikely to form ordered fibrils.

Introduction

According to the amyloid hypothesis, Alzheimer's disease (AD) is a result of deposition in brain tissues of Aβ peptides, a normal product in the amyloid precursor protein metabolism [1]. Although the final product in the AD pathogenesis is the insoluble fibril formed as a result of aggregation of Aβ peptides, recent evidence suggests that Aβ oligomers and protofibrils may be the cause of neurotoxicity [2, 3, 4, 5]. Aβ oligomers have been envisioned as intermediates in the cascade of events leading to the formation of amyloid fibrils [1]. Besides AD, a number of other neurodegenerative diseases (prion disorders, Parkinson's and Huntington's diseases) are linked to amyloidogenesis [6, 7]. It is possible that, in all these cases, the mobile and soluble oligomers may be the cause of neurodegeneration. Just as in AD, the importance of neurotoxic oligomers has made it urgent to understand, at the molecular level, not only the structure of oligomers, but also the mechanisms of their assembly. In addition, given the similarity in the morphology of fibrils from a variety of peptides and proteins [8], which are unrelated in sequence or length, certain general principles governing their formation are likely to exist.

Noncrystallinity and insolubility of amyloid fibrils prevent determination of their atomic structures by conventional methods, such as X-ray crystallography or solution NMR. Nevertheless, a detailed picture of the overall architecture of the ordered fibrils is beginning to emerge from a variety of experimental techniques [9, 10]. The characteristic silk-like cross-β pattern of ex vivo amyloid propagation has been revealed by fiber X-ray diffraction studies [11]. More recently, a number of solid-state NMR studies of fibrils of both the full-length Aβ peptides and fragments have given valuable insights into the nature of β sheet organization in amyloids [12, 13]. These studies show that, in $A\beta_{10-35}$ and $A\beta_{1-40}$ fibrils, peptides form in-register parallel β sheets. On the other hand, antiparallel organization is found for the smaller fragments $A\beta_{34-42}$ [14] and $A\beta_{16-22}$ [15]. The solid state NMR measurements of the structure of amyloid fibrils formed by the fragment N-acetyl-Lys-Leu-Val-Phe-Phe-Ala-Glu-NH_2 (referred to as $A\beta_{16-22}$) revealed the antiparallel organization of these peptides [15]. This fragment, which is one of the shortest one to form amyloid fibrils, contains the crucial central hydrophobic cluster (CHC; residues 17–21, LVFFA), which has long been known to be essential for polymerization of the full-length peptide [9]. Despite the noncrystalline nature of $A\beta_{16-22}$ fibrils, the NMR lines are unusually sharp, which implies a high degree of structural order [15]. Using ^{13}C chemical shift data and direct measurements of interpeptide distances between ^{13}C- and ^{15}N-labeled CO and NH atomic groups, Tycko and coworkers showed that $A\beta_{16-22}$ peptides are arranged in an antiparallel manner in the fibrils [15].

$A\beta_{16-22}$ is an attractive model system to probe the mechanism of fibril assembly. Unlike the fibers of larger fragments, the structure of $A\beta_{16-22}$ fibrils may be anticipated from its sequence alone. The interpeptide interactions must be dominated by favorable contacts between CHC hydrophobic residues. Antiparallel registry confers additional stability by forming interpeptide salt bridges between Lys16 and Glu22. Although the formation of β-helical fibers [16], even for this short peptide, cannot be ruled out, the present study suggests that such structures have higher free energies than the antiparallel structures.

Knowledge of fibril structure, while important, does not provide insights into the assembly mechanism. Therefore, it is essential to study the structural changes in the transition from the monomer to the fibrils at an atomic level. Toward this end, we present, for the first time, the study of oligomer formation for interacting $A\beta_{16-22}$ peptides and their variants using all-atom molecular dynamics (MD) simulations [17]. Several relatively long MD trajectories were used to establish the kinetics of $A\beta_{16-22}$ assembly into antiparallel β sheets. The observation that even a small number of $A\beta_{16-22}$ peptides form antiparallel structures suggests that the size of the critical nucleus for fibrillization cannot be very large. Surprisingly, simulations suggest that α-helical structures represent obligatory intermediates, even though the monomers themselves have a very low propensity to

*Correspondence: thirum@glue.umd.edu (D.T.), klimov@glue.umd.edu (D.K.K.)

Key words: amyloid peptide; oligomer; α-helical intermediate; antiparallel β sheet; Alzheimer's disease

form α-helical conformations. We argue that the mechanism outlined here may be general in the oligomerization of Aβ peptides. Our study shows that the initial driving force for oligomer formation is hydrophobic interaction between the residues in the CHC. Antiparallel registry requires proper orientation of the charged residues. Using these findings we suggest that the structural models of Aβ peptides in the fibrils may be obtained by maximizing the number of hydrophobic interactions and salt bridges. Our results also imply that the replacement of Lys16 and Glu22 by polar residues would disrupt fibrillization.

Results

$A\beta_{16-22}$ Monomers Adopt Random-Coil or β Strand-like Structures

To understand the dynamics of assembly of Aβ oligomers, we must first characterize the structure of Aβ monomers. There are no solution structures of $A\beta_{16-22}$ at neutral pH. The solution NMR structure of $A\beta_{10-35}$ (Protein Data Bank code 1hz3, T = 283°C, pH = 5.6) suggests that it adopts a compact random-coil (RC) conformation [18]. According to the DSSP secondary structure assignment, none of the residues in the segment 16–22 of $A\beta_{10-35}$ are in α helix or β strand conformations. A direct probe of the structure of the monomer $A\beta_{16-22}$ is needed, especially because it is the sequence context that determines the nature of secondary structures. Moreover, structural characteristics of the monomer will serve as a suitable reference for the conformational changes that take place in the process of oligomerization.

To characterize the conformational states of the $A\beta_{16-22}$ monomer, we generated eight 8 ns trajectories. Using the definitions for conformational states of peptides (see Experimental Procedures), we established that RC and β strand conformations constitute 68% and 29% of all monomer structures, respectively. The population of α helix peptide conformations is negligible (3%). These results are consistent with the simulations of $A\beta_{10-35}$ monomers, in which the CHC was found to have some β strand propensity [19].

The time dependence of β strand, $<S(t)>$, and α helix, $<H(t)>$, contents (see Equation 1 in Experimental Procedures) are shown in Figure 1A. The population of RC residue states may be obtained with the equation $<R(t)> = 1 - <S(t)> - <H(t)>$. The time-averaged values of the populations of β strand and α helix residues in the monomers are 0.33 and 0.11, respectively. Thus, the monomer exists predominantly in the RC or β strand state. The residue-specific α helix, $P_h(i)$, and β strand, $P_s(i)$, propensities show (Figure 1B) that β strand conformations are clearly preferred at Val18, which is consistent with the Chou-Fasman prediction [21]. The snapshots of the typical monomer conformations are shown in Figure 1C.

Interpeptide Hydrophobic Interactions Drive Formation of $A\beta_{16-22}$ Oligomers

To probe the effect of interpeptide interactions on the dynamics of secondary structure, we generated four 11 ns trajectories for the solvated system of three $A\beta_{16-22}$ peptides (Figure 2A). Time dependence of the radii of gyration, R_{gi}, (Figure 2B) shows that interpeptide interactions lead to large changes in the size of the peptides. Although the initial values of R_{gi} are below 8 Å (R_g of the monomer is about 8.6 Å), interactions between peptides cause a dramatic increase in peptide dimensions. For example, by the end of the trajectory shown in Figure 2B ($t \approx 8$ ns), $R_{g2} \approx 11$ Å, which constitutes nearly a 50% increase in about 8 ns. The dimensions of one of the peptides (labeled 3 in Figure 2B) do not change as dramatically, which is perhaps a consequence of relatively weak interactions with other peptides. Thus, peptides in oligomers become extended as a result of interpeptide interactions.

The secondary structure changes (Figure 2C) accompanying the peptide extension give a preliminary view of the assembly mechanism of the oligomers. Shortly after initial equilibration α-helical conformations dominate in all peptides (Figure 2C, red regions). Subsequently, a rather dramatic increase in the β strand content (shown in Figure 2C, green) is observed, indicating α → β conversion. For example, up to 2 ns, none of the residues in peptide 2 (Figure 2C) are in β strand conformations ($S_2 \approx 0$), while a persistent α helix structure is seen at Val18, Phe19, and, to a lesser extent, at Ala21. In the time interval from 2 to approximately 4 ns, β strand conformations emerge at positions Leu17, Val18, and, subsequently, Phe20, while the α-helical structure survives only at Ala21. Transition to β strand conformation also occurs later at Phe19 (Figure 2C). Consequently, the β strand content, $S_2(t)$, reaches a remarkably high value of 0.8 at about 7 ns. Significantly, α → β transition is also observed in peptide 1. The amount of β strand content in peptide 3, $S_3(t)$, remains small. The average β structure content in all three peptides in this trajectory approximately doubles. The increases in S_1 and S_2 are consistent with the changes in the radii of gyration, R_{g1} and R_{g2}, in Figure 2B. Similar dramatic α → β transition occurs in other trajectories on a similar timescale (data not shown).

To probe the orientations of peptides in $A\beta_{16-22}$ oligomers, we computed the functions, $d_{ij} = (\hat{u}_i\hat{u}_j)$, for each pair of peptides, where $\hat{u}_i$ is the end to end unit vector of ith peptide. Rapid variations in d_{ij} (data not shown) on timescales as short as 1 ns indicate frequent reorientations of peptides in Aβ oligomers. For this reason, we refer to such trimer structures as disordered oligomers.

Dynamics of α → β Transition

The time dependence of the β strand (α helix) structure content in a peptide, $<S(t)>(<H(t)>)$, shows a striking behavior (Figure 3A). The β strand content, $<S(t)>$, increases monotonically (apart from relatively minor fluctuations), while $<H(t)>$ decreases. Initially, the α-helical content in the peptides is more than four times higher than the β strand population. In about 11 ns, the β strand population reaches 0.40, while the α helix content falls below 0.10 (Figure 3A). Thus, in the course of oligomer formation, a dramatic conformational change in the peptides is observed, as illustrated in Figure 3B.

Because there are only three peptides in our simulations, we expect large fluctuations in the oligomer struc-

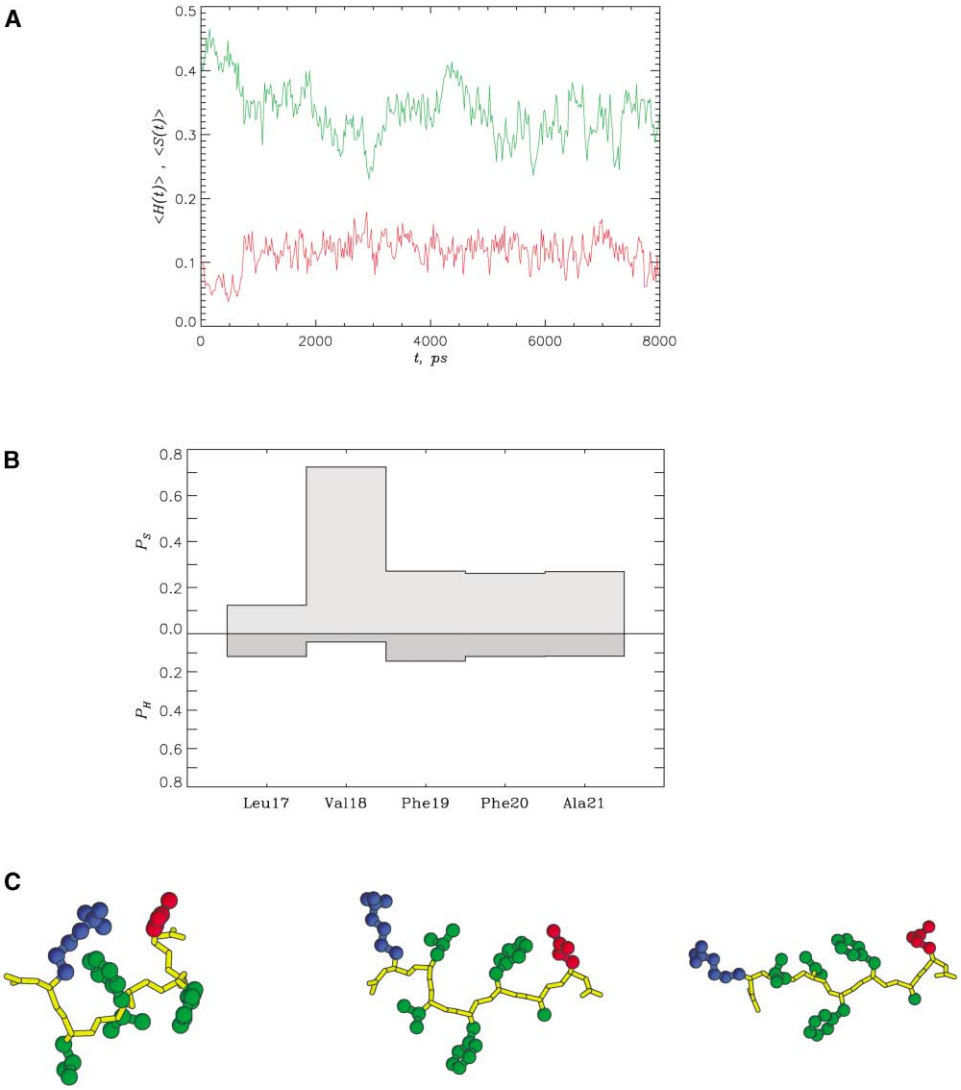

Figure 1. Characteristics of Aβ16–22 Monomers

(A) The average β strand, $<S(t)>$, (green) and α helix, $<H(t)>$, (red) contents in Aβ16–22 monomers as a function of time. $<S(t)>$ and $<H(t)>$ give the probability to observe a residue in a β strand or α helix conformation averaged over the ensemble of eight independent trajectories.

(B) The β strand, $P_s(i)$, and α helix, $P_h(i)$, propensities as a function of sequence position, i, in Aβ16–22 monomers. $P_s(i)$ and $P_h(i)$ are the probabilities for observing a β strand or α helix structure at i, which are averaged over eight trajectories.

(C) Representative snapshots of monomer structures. The structure on the left is in RC conformation, with zero β strand or α helix contents. The other two structures are in β strand states. Specifically, four out of five residues are in β strand conformations in the center snapshot, while all residues in the right snapshot are in β strand conformations. If all the residues in Aβ16–22 are in β strand conformations, the end to end distance, r_{IN}, is approximately 23 Å. Because of large conformational fluctuations, r_{IN} for β strand-like structures is typically smaller than 23 Å. The charged side chains are shown in blue (Lys16) and red (Glu21), and the hydrophobic (CHC) side chains are shown in green. The program RasMol v2.6 [20] has been used to visualize molecular structures in this and other figures.

ture. Although the average β strand content reaches about 0.4, there are substantial variations in the secondary structure propensities at the residue level. Using the average probabilities to observe β strand, $P_s(i)$, or α helix, $P_h(i)$, conformations at residue i, we find that $P_s(i)$ values for Leu17, Val18, and Phe20 are 0.26, 0.41, and 0.28, respectively [the corresponding $P_h(i)$ values are 0.09, 0.31, and 0.17]. Other residues (i = Phe19, Ala21) are better accommodated by an α-helical structure [$P_h(i) > P_s(i)$]. The ratio $P_s(i)/P_h(i)$ is 1.4, which reflects the general bias toward β strand conformations in Aβ peptides. The largest β strand propensity is found for Val18, which may be identified as the initiation site for the β strand structure. We can also surmise that, during aggregation of Aβ16–22, β strand formation begins near the peptide's N terminus.

Using the definitions for α helix and β strand peptide structures (see Experimental Procedures), we determined that the Aβ16–22 peptide in the oligomer adopts β strand and α helix states, with the probabilities 0.30 and 0.26, respectively. The probability of finding a peptide in a random-coil state is 0.44. Thus, β strand and α helix states together constitute more than half of all peptide conformations.

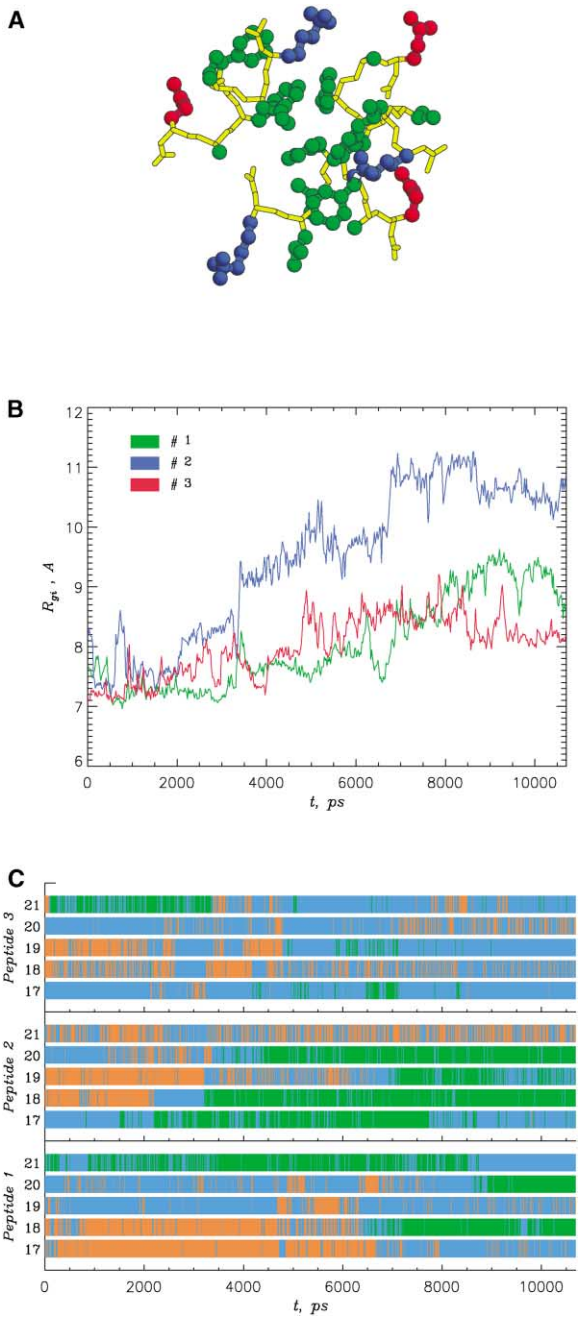

Figure 2. Structural Features of $A\beta_{16-22}$ Disordered Oligomers

(A) The snapshot of the solvated $(A\beta_{16-22})_3$ oligomer. Residues are colored as in Figure 1C. The oligomer is stabilized by mostly hydrophobic interactions between CHC residues (green). Because salt bridges are rare, the peptides do not show any preferential orientations in the oligomer. We refer to such an oligomer as disordered, as opposed to that observed on longer timescales (Figure 4B). For clarity, water molecules are not shown.

(B) The radii of gyration of peptides, R_{gi}, as a function of time for one of the $(A\beta_{16-22})_3$ trajectories. Colors encode peptides as indicated in the plot.

(C) Dynamics of secondary structure in $A\beta_{16-22}$ peptides forming an oligomer at the residue level (same trajectory as in [B]). The secondary structure is assigned according to the values of dihedral angles ϕ and ψ (see Experimental Procedures). β strand, α helix, and RC conformations are represented in green, red, and blue, respectively.

The distribution of (ϕ,ψ) states in Figure 3C shows that conformational states of individual residues tend to localize near either the α helix or β strand states. The plot identifies a region to the left of the α helix state, which also has a significant population (an RC state). The α helix and β strand states are connected by a path, which is apparently sampled during the α helix → β strand conversion. This observation is consistent with Figure 3A, which demonstrates that the increase in the β structure content occurs at the expense of α helix states.

Assembly of Ordered $A\beta_{16-22}$ Oligomers

Disordered oligomers are stabilized by an extensive network of interpeptide hydrophobic interactions. Despite occasional interpeptide contacts between charged Lys and Glu residues, a stable antiparallel β sheet arrangement is not discernible on the timescale of the simulations (~11 ns). To enable the formation of antiparallel β sheet structures on simulation timescales, we adopted a "fast-forward" strategy to probe the assembly of the ordered oligomer (see Experimental Procedures). Our strategy targets the dynamics of "successful" oligomer formation at longer timescales.

There are large variations in the kinetics of ordered oligomer assembly, which are indicative of heterogeneity of assembly pathways. For example, residues in peptides 1 and 3 frequently sample β states, whereas peptide 2 is predominantly α helical (data not shown). The highest β strand content is found in peptide 1 ($\langle S_1 \rangle$ = 0.35). For comparison, in peptide 2, $\langle S_2 \rangle$ = 0.05. In accord with this, the average radii of gyration for peptides 1 and 3, $\langle R_{g,1} \rangle$ = 9.0 Å and $\langle R_{g,3} \rangle$ = 8.8 Å, are larger than that for helix-rich peptide 2 ($\langle R_{g,2} \rangle$ = 7.7 Å). In contrast, in another trajectory for the ordered oligomer, the α helix structure in peptide 2 almost completely dissolves after about 1.5 ns and is converted to β strand conformations. Simultaneously, an increase in $R_{g,2}$ from 7.5 Å to 9.0 Å is observed. This structural transition results in small α helix content ($\langle H_2 \rangle$ = 0.14). The probability of finding a peptide in the $A\beta_{16-22}$ ordered oligomer in the β strand state (average over four trajectories) is 0.40. Strikingly, the probability of finding α helix peptide states is much smaller (0.19). The probability of finding random-coil peptide states (0.41) is comparable to that for β strand states.

Antiparallel Registry of Peptides in $A\beta_{16-22}$ Oligomers

The emergence of antiparallel β sheets is most clearly seen if one examines $d_{ij} = \hat{u}_i(t)\hat{u}_j(t)$ (see Experimental Procedures). For an ideal antiparallel arrangement of the peptides i and j, $d_{ij} = -1$, while $d_{ij} = 1$ if the peptides are in parallel conformation. We found that, in one of the trajectories, two pairs of peptides (labeled 1-2 and 1-3) rapidly (in about 1 ns) adopt antiparallel orientations, while peptides 2 and 3 are parallel (Figure 4A). Once such a structure is formed, it remains mostly stable during the course of simulations (~6 ns). Interpeptide

A dramatic conversion of an α helix structure into a β strand in peptide 2 is correlated with its extension (see text for details).

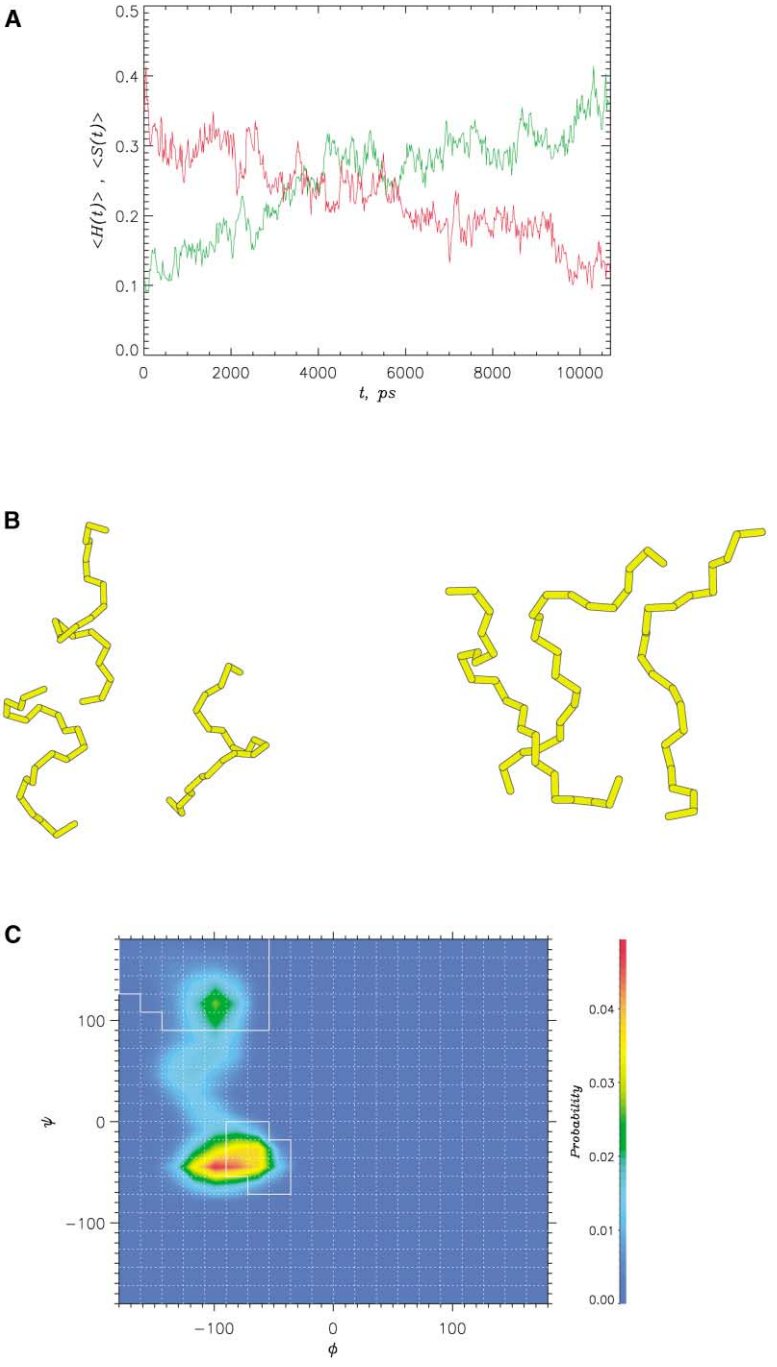

Figure 3. Interpeptide Interactions Drive α Helix → β Strand Transition

(A) The average β strand, $<S(t)>$, (green) and α helix, $<H(t)>$, (red) contents in Aβ16–22 peptides in disordered oligomers as a function of time. $<S(t)>$ and $<H(t)>$ give the probability for observing a residue in a β strand or α helix conformation averaged over the ensemble of four independent trajectories. The plot shows α → β transition, which is driven by extensive (mostly hydrophobic) interpeptide interactions.

(B) The backbone traces of Aβ16–22 oligomers illustrate the α → β structural transition shown in Figure 3A. Approximately two-thirds of residues in the left oligomer are in α helix conformations, and none adopt β strand states (other residues are in RC conformations). The structure is taken at 43 ps (soon after the start of the production run). In the snapshot on the right, recorded about 10 ns later, two-thirds of residues are already in β strand conformations, whereas the fraction of α helix residues is dropped to less than 0.1.

(C) Distribution of (ϕ,ψ) dihedral angles in the disordered Aβ16–22 oligomers. The 18° interval grid is shown by white dashed lines. The α helix and β strand states are contoured with solid white lines. Residue conformations in Aβ16–22 oligomers are restricted to α helix, β strand, and RC (next to α helix) states. The path connecting the α helix and β strand regions is attributed to α → β transition.

salt bridges between Lys16 and Glu22 confer stability to the pairs of peptides in antiparallel registry. Stable electrostatic contacts between Glu and Lys of the peptides pairs 1-3 and 2-3 (with the probabilities $P_{1\text{–}3,Glu22\text{-}Lys16} = 0.94$ and $P_{1\text{–}2,Glu22\text{-}Lys16} = 0.64$) ensure proper orientation in antiparallel β sheets. An example of antiparallel in-registry packing of peptides 1 and 3 in Aβ16–22 oligomers is shown in Figure 4B.

Taking into account the most frequent contacts and the functions, d_{ij}, for each trajectory, we reconstruct preferential orientation of peptides in Aβ16–22 oligomers and the network of frequent interactions between peptides 1 and 2 and peptides 1 and 3 (Figure 4C). This figure illustrates that the antiparallel orientation of Aβ16–22 peptides is determined by electrostatic contacts between charged terminals. For peptides 1 and 2, the contact Glu22-Lys16 stabilizes the formation of (mostly) hydrophobic contacts Phe19-Lys16, Phe19-Phe20, and Leu17-Phe20. For peptides 1 and 3, the contact between charged terminals Lys16-Glu22 (the opposite terminal in the peptide 1) serves to stabilize the antiparallel registry of this pair of peptides. Besides the salt bridge, the antiparallel pattern of contacts between peptides 1 and 3 is established by Leu17-Ala21, Leu17-Phe20, Phe19-

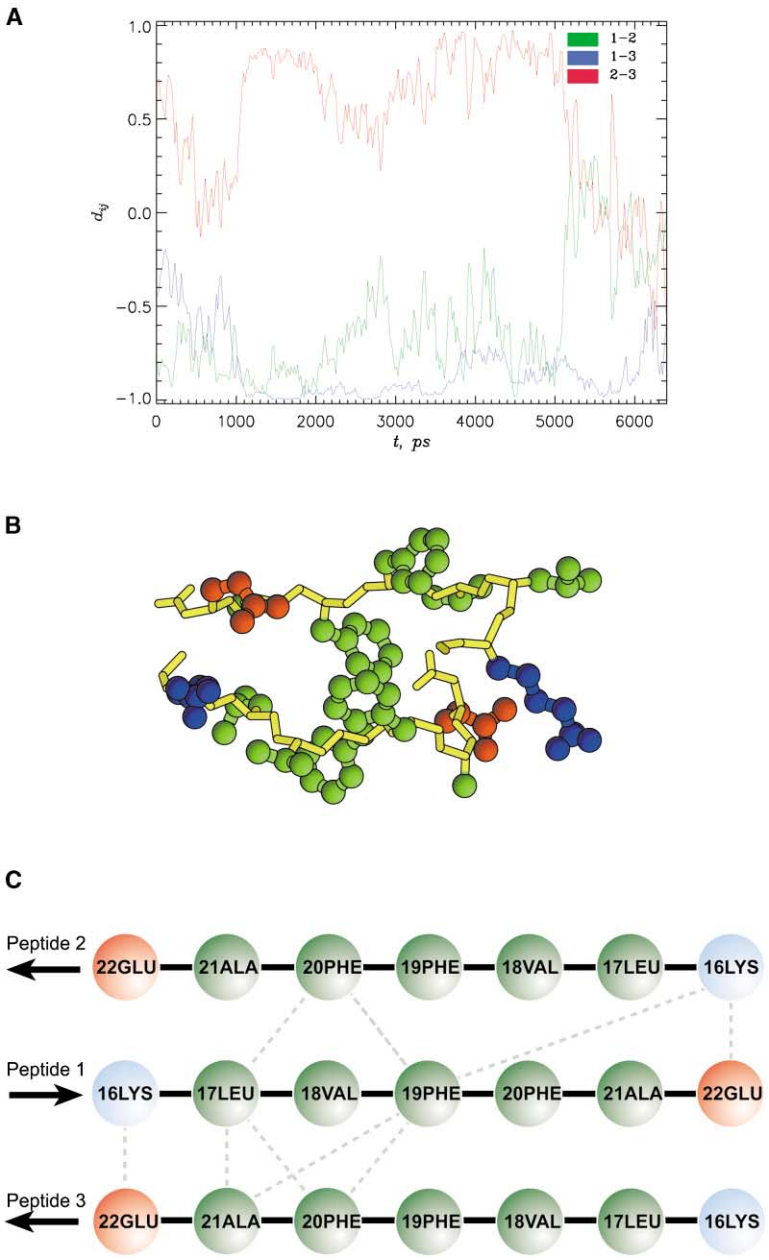

Figure 4. Antiparallel Registry of $A\beta_{16-22}$ Peptides

(A) Orientations of peptides in ordered $A\beta_{16-22}$ oligomer characterized by the time dependence of $d_{ij} = (\hat{u}_i\hat{u}_j)$ (see Experimental Procedures for definition). Colors code peptide pairs. Analysis shows that peptides 1 and 3 maintain an almost perfect antiparallel in-registry orientation for at least 5 ns. Note that the interaction between peptides 1 and 2 is weak.

(B) The conformational snapshot for peptides 1 and 3, which are locked in antiparallel in-registry packing. Two salt bridges between charged terminals Lys and Glu (blue and green, respectively) are formed in this structure. Side chains are colored as in Figure 1C.

(C) The emerging antiparallel registry of peptides in ordered $A\beta_{16-22}$ oligomers illustrated through the network of most-frequent interpeptide contacts (gray dashed lines). The interpeptide interactions propagate from the anchoring contacts between charged side chains Lys16 and Glu22, which establish antiparallel orientation of peptides.

Ala21, and Phe19-Phe20. The electrostatic interactions confer the required specificity to form in-register peptide packing. Because the contacts between peptides 2 and 3 are weak (their average probability is less than 0.50) and less numerous, peptide 1 acts as a linker between peptides 2 and 3. We believe that the observed antiparallel pattern represents the initial seed, which, in the presence of other peptides, may subsequently grow into amyloid fibrils.

Because assembly of the $A\beta_{16-22}$ oligomer takes place in the solution, there are considerable fluctuations as compared with the fibrils monitored in solid-state NMR [15]. As a result the β strand content in oligomers is not nearly as large as that observed in fibrils [15]. Nevertheless, the tendency to form antiparallel β sheets with substantial β strand content is established in our simulations. Although the number of successful formations of antiparallel β sheets is relatively small, it is clear that the structures of interacting peptides in oligomers resemble those that are formed in fibrils.

β *Helix Formation for* $A\beta_{16-22}$ *Peptides Is Unlikely*

On the basis of electrostatic considerations alone, we can assess the formation of a circular arrangement of the $A\beta_{16-22}$ peptides. In fact, such structures, in which the charged terminals of one peptide are in contact with the terminals of two other peptides, were transiently observed in our simulations. Such an oligomer can be a seed for forming a β-helical fiber [16], in which the

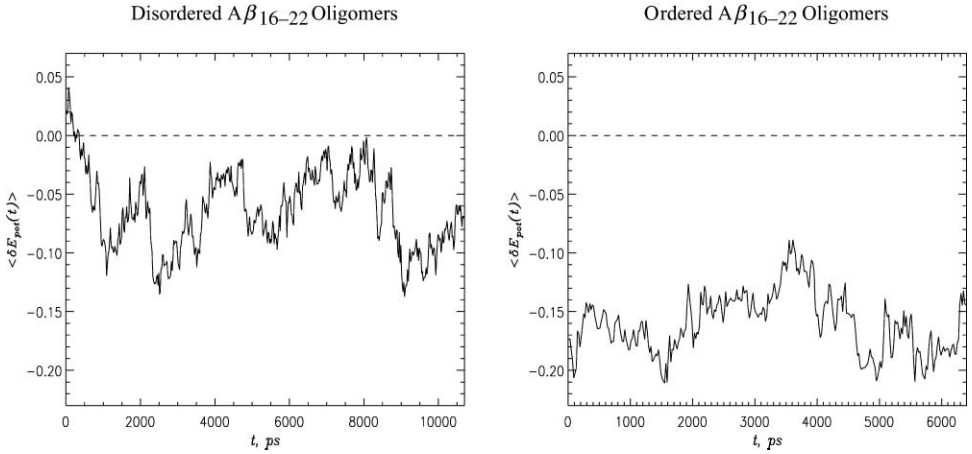

Figure 5. Energetics of Oligomerization

The time dependence of the relative potential energy, $<\delta E_{pot}(t)>$, for the disordered (left panel) and ordered (right panel) oligomers. The dashed baseline indicates the relative potential energy of an $A\beta_{16-22}$ monomer. The panels show that formation of oligomers is energetically favorable. Additional gain in stability due to electrostatic interactions lowers the average $<\delta E_{pot}(t)>$ for an ordered oligomer as compared with a disordered oligomer.

orientation of each tripeptide unit is opposite to those of its immediate neighbors. Our current simulations suggest that circular oligomers are unstable, because the interpeptide hydrophobic interactions are compromised. The formation of a circular conformation stabilized by both interpeptide salt bridges and hydrophobic interactions that can propagate to a β-helical fiber structure requires at least six peptides. Therefore, such arrangement cannot be ruled out on the basis of the present simulations alone. Note that formation of β-helical structures also places like charges at the vertices of the tripeptide triangles, and, hence, β helices are likely to be unstable. Additional experiments are needed to rule out the possibility of β helix formation for this class of peptides.

Interactions Contributing to the Antiparallel β Structure

Figure 5 shows that the formation of $(A\beta_{16-22})_3$ is energetically favorable. This follows from the time dependence of $<\delta E_{pot}(t)> = (<E^o_{pot}(t)> - 3<E^m_{pot}>)/3<E^m_{pot}>$, where $<E^o_{pot}(t)>$ is the potential energy of the oligomer averaged over four trajectories and $<E^m_{pot}>$ is the time-averaged potential energy of the monomer. This plot clearly shows that, because of favorable electrostatic interactions, the antiparallel arrangement of peptides provides an additional gain in stability as compared with the disordered oligomer [22]. The importance of electrostatic interactions can also be gleaned from the fluctuations in the potential energy, $E^o_{pot}(t)$, of the $A\beta_{16-22}$ oligomer. Dramatic fluctuations in $E^o_{pot}(t)$ are associated with the formation and dissolution of contacts between charged residues. A strong correlation (the average correlation factor is 0.8) is observed between $E^o_{pot}(t)$ and the number of interpeptide salt bridges between Lys and Glu. In contrast, no correlation (the average correlation factor is 0.1) is seen between $E^o_{pot}(t)$ and the total number of interpeptide hydrophobic contacts. Therefore, electrostatic interactions play a crucial role in the orientation of the peptides, while hydrophobic interactions provide a nonspecific "glue" for binding $A\beta_{16-22}$ peptides together.

The assembly dynamics also suggests that electrostatic and hydrophobic interactions play distinct roles in antiparallel β sheet formation. The extent to which hydrophobic and electrostatic interactions control the assembly of oligomers is not only relevant for understanding the initial events in $A\beta_{16-22}$ oligomerization, but also in the context of fibrillogenesis of full-length Aβ peptides.

To probe the distinct role of electrostatic and hydrophobic interactions, we engineered two mutants. In one of them, labeled K16G/E22G, the charged residues Lys16 and Glu22 are replaced with polar and neutral Gly. This substitution eliminates the possibility of formation of interpeptide salt bridges. In the second mutant, L17S/F19S/F20S, we substituted three hydrophobic residues, Leu17, Phe19, and Phe20, with polar Ser. These positions are chosen because most of the hydrophobic interpeptide contacts in $A\beta_{16-22}$ oligomers involve these amino acids. By studying the assembly of the mutated peptides, we can dissect the role of electrostatic and hydrophobic interactions. For both the mutants, we generated four independent trajectories using the initial wild-type structures for the ordered oligomer.

K16G/E22G $A\beta_{16-22}$

The principal result obtained for this mutant is that the oligomer becomes unstable. In three (out of four) trajectories, dissolution of peptides is observed. As an example, we display, in Figure 6A, the distances between peptides centers of mass, R^{CM}_{ij}, as a function of time for one of the trajectories. Shortly before 1.5 ns peptide 1 breaks away as the distances, R^{CM}_{12} and R^{CM}_{13}, sharply increase. Accordingly, the number of interpeptide contacts, $C_{12}(t)$ and $C_{13}(t)$, drops to zero (data not shown). The breakage of peptide 1 is "permanent" because the contacts with other peptides are not restored (Figure 6B). Similar events take place in two other trajectories,

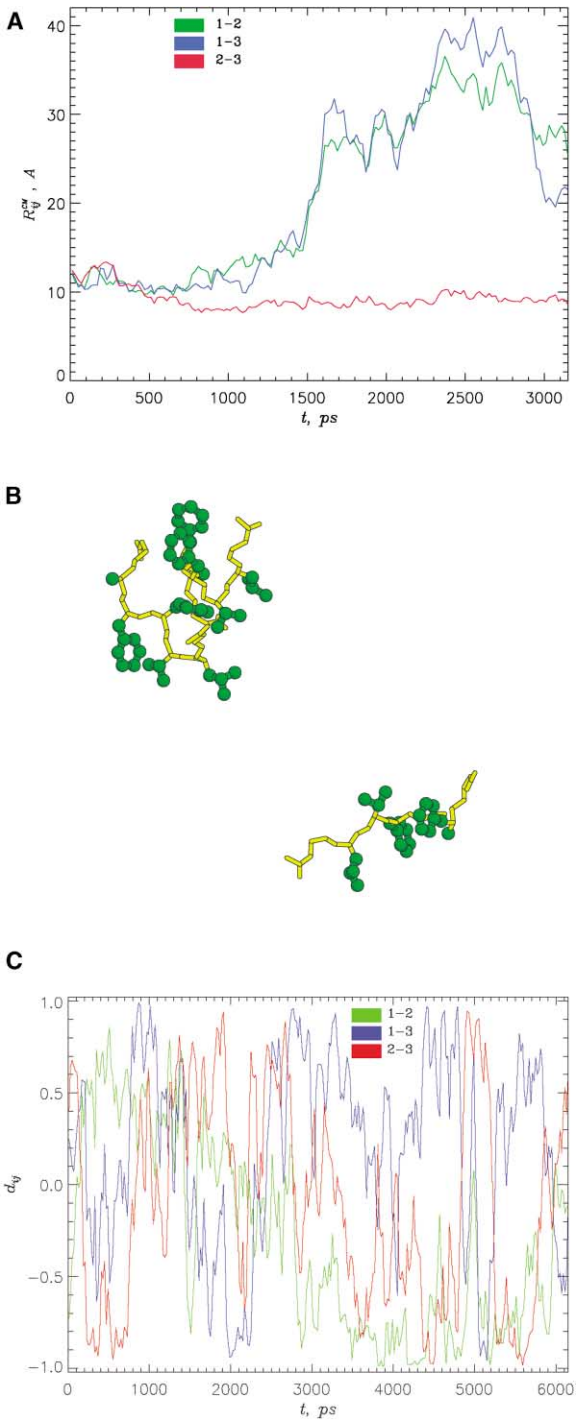

Figure 6. Structural Characteristics of the K16G/E22G Aβ_{16-22} Mutant

(A) The distances between the centers of mass of K16G/E22G Aβ_{16-22} peptides, R_{ij}^{CM}, as a function of time. Sharp increase in R_{12}^{CM} and R_{13}^{CM} reflect breaking of peptide 1 from the K16G/E22G Aβ_{16-22} oligomer at about 1.5 ns. Color-coding is as in Figure 4A.

(B) Snapshot of the final conformation for the trajectory shown in Figure 6A. After 2 ns the distance between peptide 1, which escaped from the Aβ oligomer at about 1.5 ns, is increased to about 25 Å. Hydrophobic side chains are given in green.

(C) The time dependence of $d_{ij} = (\hat{u}_i\hat{u}_j)$ (see Experimental Procedures for definition) for the K16G/E22G Aβ_{16-22} oligomer. d_{ij} quantifies the orientations of peptides for the trajectory, in which oligomer integrity was retained. Frequent variations in d_{ij} are in sharp contrast with the almost constant values of d_{ij} seen for the ordered oligomer (Figure 4A). On average, the fluctuations in d_{ij} are twice as large for K16G/E22G as compared with the wild-type. Color-coding is as in Figure 4A.

as well. Although we cannot rule out aggregation of AβK16G/E22G on much larger timescales, the stability of such a structure would be considerably less than that for the wild-type oligomers. Dynamics of $d_{ij}(t)$ show that deletion of charged terminals significantly increases the fluctuations in the orientations of peptides in the Aβ_{16-22} oligomer (Figure 6C). The peptides frequently change their orientations relative to each other, and, in many instances, reverse it by 180°. Thus, replacing charged terminals with polar residues produces a drastic destabilizing effect on Aβ_{16-22} oligomers.

L17S/F19S/F20S Aβ_{16-22}

In all the trajectories, we observed partial dissolution of amyloid oligomers for this mutant. For example, in one of the trajectories, peptide 3 breaks away at about 0.9 ns as the distances between the centers of mass, R_{13}^{CM} and R_{23}^{CM}, exceed 15 Å (Figure 7A), and the number of contacts that peptide 3 forms with other chains drops to zero. After peptide 3 separates from the trimer, the distance between peptides 1 and 2, R_{12}^{CM}, also gradually increases up to 20 Å. At this point the only contact (between charged terminals Glu22 and Lys16) remains intact between these peptides (Figure 7B). Separation of peptides from the oligomer is also observed in all other trajectories.

The simulations of the L17S/F19S/F20S mutant provide strong evidence that the removal of three hydrophobic residues makes Aβ_{16-22} oligomers unstable. Not only did we observe individual peptides separating from oligomers, but the entire oligomer complex itself became loosely formed and, in a few instances, appeared to be on the brink of disintegration. Overall, we registered four events, in which Aβ_{16-22} peptides break away from oligomers on an approximately 13.9 ns total timescale.

Replacement of three bulky hydrophobic residues with a relatively compact polar Ser drastically affects the β strand and α helix propensities, as well. The average β strand residue content in this mutant ($<S> = 0.19$), is smaller than the population of α helix residues ($<H> = 0.28$). The α helix propensity is especially large at the positions Ser19 and Ser20 [$P_h(Ser19) = 0.54$ and $P_h(Ser20) = 0.46$]. The corresponding β strand propensities are about 0.1. The dominance of α helix structures is the direct consequence of sequence mutation, which reduces steric constraints.

By comparing the results for the wild-type and the two mutants, we draw two important conclusions: (1) both hydrophobic and electrostatic interactions are crucial for the assembly of Aβ_{16-22} into an ordered oligomer, and (2) the initial driving force of oligomer assembly is favorable interpeptide interaction between the LVFFA cluster. However, the ordered (antiparallel) orientation is only obtained upon the formation of salt bridges. The latter imparts the stability to antiparallel conformations of peptides as evidenced by $d_{ij}(t) \approx -1$ (Figure 4A). In accord with this we find that the orientational fluctua-

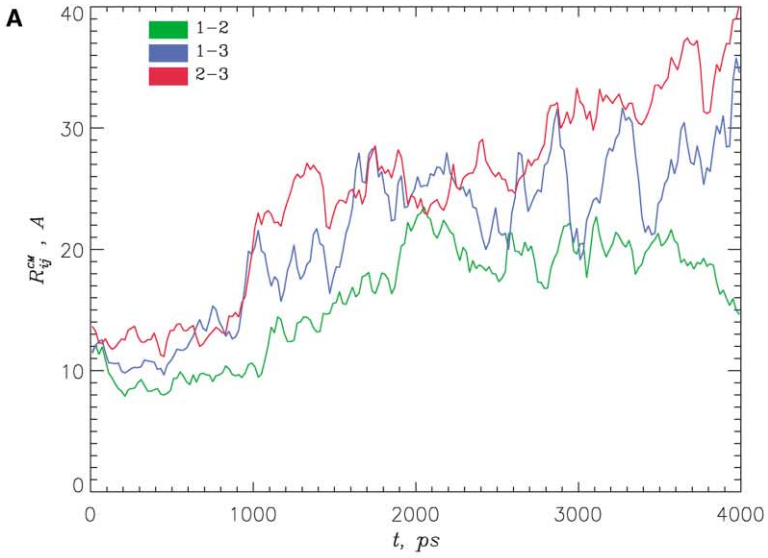

Figure 7. Conformational Characteristics of the L17S/F19S/F20S Aβ16–22 Mutant

(A) The distances between the centers of mass of L17S/F19S/F20S Aβ16–22 peptides, R_{ij}^{CM}, as a function of time. An increase in R_{ij}^{CM} reveals partial dissolution of the oligomer, starting with the separation of peptide 3 from the oligomer at ~0.9 ns. By the end the trajectory the interactions between peptides 1 and 2 are also weakened. Color-coding is as in Figure 4A.

(B) Snapshot of the final conformation in the trajectory shown in Figure 7A. By 4 ns peptide 3 is 35 Å apart from two other peptides, which are only linked by a single salt bridge. Side chains are colored as in Figure 1C, except for Ser side chains (orange).

tions are considerably less for the AβL17S/F19S/F20S mutant than in AβK16G/E22G.

So far we have focused on the contributions of salt bridges and hydrophobic interactions to the stability of peptides in Aβ16–22 oligomers. On the other hand, by using ^{13}C- and ^{15}N-labeled Aβ16–22 peptide samples, Balbach et al. [15] concluded that a hydrogen bond is established between CO(Leu17) and NH(Ala21). We investigated hydrogen bonding in Aβ16–22 oligomers and found that the hydrogen bond NH(Leu17)-CO(Ala21), which has the highest probability of occurring in the simulations, is also formed between these residues. When this hydrogen bond is present, the average distance between nitrogen and carbonyl atoms is 4.4 Å, which is consistent with the antiparallel arrangement of peptides [15]. However, because simulations are performed in water, we observe frequent disruptions in hydrogen bonding. The few interpeptide hydrogen bonds that are frequently formed are largely localized near the stable interpeptide side chain contacts.

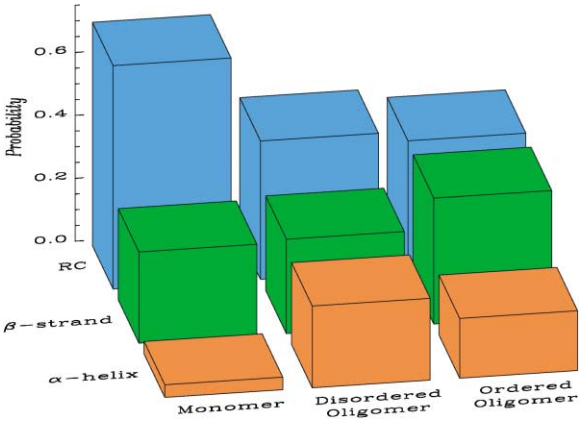

Figure 8. The Distribution of $A\beta_{16-22}$ Peptide Conformational States for the Monomer, Disordered Oligomer, and Ordered Oligomer

The plot demonstrates that monomer conformations are predominately RC (blue) or β strand (green). In the course of oligomer assembly, the share of β strand conformations increases, whereas the fraction of the α-helical states (red) reaches maximum in disordered oligomers and declines with oligomer ordering (propagation of antiparallel registry). The RC states become less populated with the progress in oligomer assembly. The occurrence of α-helical intermediates and the accumulation of β strand structures are consistent with recent experiments [11].

Discussion

Assembly Mechanism—Road to Antiparallel β Sheet Is through α-Helical Intermediate

Multiple long molecular dynamics simulations of interacting $A\beta_{16-22}$ peptides yield novel insights into the plausible mechanisms governing oligomerization. The conformations of $A\beta_{16-22}$ peptides, in a monomeric form, partition into two distinct sets of structures. The first consists of RC conformations with the mean end to end distance typical of collapsed peptides. The second is best described by extended β strand-like conformations. The small size of this peptide allows for frequent transitions between those structures on the simulation timescale. The strongest propensity to form a β strand is found for Val18. Somewhat surprisingly the α-helical structures are rarely sampled by monomers.

Relatively little is known about the mechanisms of oligomerization. The timescale for forming detectable oligomers (or fibrils) of even short fragments of Aβ peptides is too long to be directly probed by MD simulations. Nevertheless, MD can give a glimpse of the initial events in the assembly of Aβ peptides into ordered structures. Out of the four trajectories totaling more than 40 ns for the wild-type, only one is clearly found to have an antiparallel arrangement of Aβ peptides. Multiple simulations starting from such structures established that this arrangement, once formed, is stable. However, in all the trajectories, a profound conformational transition from α-helical to β strand structures is observed, which is driven by interpeptide interactions. Even for this short fragment, the α-helical conformations are (initially) preferentially populated. Significantly, such a structural transition is not seen for $A\beta_{16-22}$ monomers. Our simulations clearly reveal a gain in β strand content and a transient increase in α helix content (Figure 8). These observations are reminiscent of the aggregation dynamics of full-length Aβ peptides [11]. Because an α-helical population is always detected for interacting peptides regardless of the initial conditions, we propose that the α-helical structure is an obligatory intermediate in the process of oligomerization. Thus, the plausible kinetic mechanism for the assembly of Aβ oligomers, which involves multiple pathways, may be described by the following scheme.

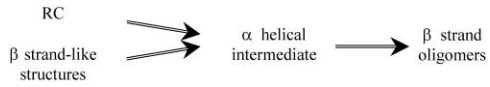

The mobile β strand oligomers can grow to form insoluble fibers either by nucleated polymerization [23] or templated assembly [24].

To gain further insight into the structure of $(A\beta_{16-22})_3$, we have computed the radial distribution of water molecules around $A\beta_{16-22}$ oligomers. Surprisingly, we found that the density of water is substantially reduced in the interior of the oligomer as compared with the bulk value (data not shown). Moreover, near its center, the $A\beta_{16-22}$ oligomer is effectively dehydrated. Eisenberg and coworkers [25] have shown that a peptide from yeast prion Sup35 also forms dry β sheet amyloids. Therefore, it appears that expulsion of water may not be the rate-limiting step in the assembly of oligomers for these relatively short fragments.

Recently, by monitoring secondary structure changes by circular dichroism, Teplow and coworkers [11] showed that, at the first stages of assembly of amyloids, the $A\beta_{1-40}$ and $A\beta_{1-42}$ peptides adopt helical conformations. Only subsequently does the $\alpha \rightarrow \beta$ transition take place. These findings suggest that α-helical conformations may be "on-pathway" intermediates to fibrillization. Their detailed experimental observations and our MD simulations (on much shorter timescales) suggest that, at least in this class of peptides, multiple routes to amyloid fibrils with obligatory α-helical intermediates may represent a general mechanism. A plausible rationalization for this conclusion can be given as follows. Our simulations clearly show that the major driving force for oligomerization is hydrophobic interaction, which serves as glue for the peptides. Initially, a given peptide interacting with the others finds itself in a confined region that is predominantly hydrophobic. The interaction-driven hydrophobic collapse of the chains reduces the amount of volume available per peptide. Thus, the chain entropy is reduced compared with that of the structures at infinite dilution. To compensate for the loss in conformational entropy, the peptides, in a confined space, adopt appropriate low-energy structures. For Aβ peptides with relatively long stretches of hydrophobic residues, the hydrophobic collapse results in α-helical conformations. Because the helical structures cannot pack efficiently to maximize favorable interpeptide hydrophobic interactions, an $\alpha \rightarrow \beta$ transition occurs on longer timescales.

This argument suggests that the degree of confinement depends on the peptide concentration. As a result the extent of α helix formation and the timescale (t_{max} in the study of Teplow and coworkers [11]) at which the

maximum helicity is observed will depend on the peptide concentration.

It is interesting to speculate on the nature of the plausible intermediate that may be found for the $A\beta_{1-40}$ and $A\beta_{1-42}$ peptides on the basis of our studies. The N terminus of these peptides is largely hydrophilic, whereas the C terminus and 17–21 (LVFFA) CHC region are hydrophobic. The CHC region is connected to the C terminus by the VGSN turn (residues 24–27). Assuming that hydrophobic forces drive oligomerization, we propose that the structure in the intermediate is of the form RC-α-T-α, where the random coil is restricted to the hydrophilic N terminus (residues 1–10 or 12) and the turn T corresponds to the VGSN segment. The transition from this structure to a nucleus composed of β strands may be the rate-limiting step in fibrillization.

Predictions for Related $A\beta_{16-22}$ Fragments

One of the important results of our study is the distinct roles of the hydrophobic and electrostatic interactions in the formation and stabilization of the antiparallel β sheet structure of $A\beta_{16-22}$ oligomers. The initial driving force is the nonspecific association between the CHC residues. Formation of the salt bridges, Lys-Glu, not only enhances the oligomer stability, but also produces the specific antiparallel registry of $A\beta_{16-22}$ peptides. These observations can be used to predict the plausible outcomes of oligomer formation for the sequence KLVFFAX, where X is a substitute residue. Such fragments occur in alloforms of Aβ peptides. For example, the alloforms in which X is Gly, Gln, or Lys are referred to as Arctic (E22G), Dutch (E22Q), and Italian (E22K) mutants, respectively. The simulations in which X and Lys are replaced by Gly show that the oligomer is unstable in the absence of favorable interpeptide salt bridges. The same line of reasoning leads us to predict that, in the alloforms mentioned above, fibril formation with antiparallel registry of the strands is unlikely in the 16–22 fragment.

Biological Implications

Growing evidence shows that oligomers of Aβ peptides might cause neurotoxicity even though the final product of amyloidogenesis is the deposition of plaques in the brain. These observations make it important to understand, at an atomic level, the kinetics of polymerization of Aβ peptides. To shed light on this issue, we have simulated oligomer formation for the fragment $A\beta_{16-22}$ peptides, which have been observed to form ordered fibrils. Molecular dynamics simulations presented here show that the route to the ordered oligomer, which is an intermediate step in the formation of the fibril, occurs through an on-pathway α-helical intermediate, just as in the fibrillogenesis of the full-length Aβ peptides [11]. These results not only indicate a common mechanism of fibrillization in this class of peptides, but also suggest that therapeutic agents that destabilize the helical intermediates might prevent oligomerization. Stability of the ordered antiparallel β sheets depends both on electrostatic and hydrophobic interactions. While interpeptide hydrophobic interactions promote nonspecific association, the formation of salt bridges confers the precise antiparallel registry of the β stands. Therefore, those mutations, which destroy the salt bridges or weaken the net hydrophobic interactions, can also inhibit fibril formation. Furthermore, the architecture of the amyloid fibrils in Aβ peptides is determined by maximizing the number of hydrophobic and electrostatic interactions. The use of this rule and the propensities of residues at specific locations might be useful in modeling the structure of amyloid fibrils.

Experimental Procedures

Simulation Details

Molecular dynamics simulations with the MOIL program [26] were performed to probe the mechanism of oligomerization of $A\beta_{16-22}$ peptides. Specifically, we simulate the assembly of the $(A\beta_{16-22})_3$ oligomer from three $A\beta_{16-22}$ peptides. The amino acid sequence of $A\beta_{16-22}$ is Lys-Leu-Val-Phe-Phe-Ala-Glu and is capped with uncharged acetyl and amide groups. The $A\beta_{16-22}$ sequence includes the LVFFA central hydrophobic cluster from $A\beta_{1-42}$, and its terminal residues are oppositely charged (a positive charge on lysine and a negative charge on glutamic acid).

The initial conformation for the $A\beta_{16-22}$ monomer was extracted from the solution NMR structure for the $A\beta_{10-35}$ peptide (Protein Data Bank code 1hz3) [18]. For reference, we performed simulations to characterize the structural characteristics and fluctuations of the $A\beta_{16-22}$ monomer. The initial conformations of the trimer were obtained by replicating the individual $A\beta_{16-22}$ monomer structures in random orientations. The simulations were carried out with the microcanonical ensemble. The systems of peptides and water were enclosed in a cubic box. The number of water molecules, $\sim$1300, depended slightly on the initial orientations of the Aβ peptides. The density of water in the simulation box with the volume 41,781.9 Å^3 is approximately 0.98 g/cm^3 at 300 K. After a short relaxation of the positions of water molecules, the energy of the system was minimized with the conjugate gradient algorithm for 1000 steps. The particle Mesh Ewald method was used to compute electrostatic interactions [27]. The cutoff distances for direct electrostatic and van der Waals interactions were 12 and 9 Å, respectively. The dielectric constant was set to 1, and periodic boundary conditions were used for water. Starting with the energy-minimized structure, we linearly heated the system to 300 K during 300 ps simulations. After the heating stage, the system was equilibrated for an additional 300 ps at 300 K. The integration step of 1 fs was used in all MD simulations. At the heating and equilibration stages, velocities were rescaled for every interaction step. Rescaling was turned off during production runs. Conformational snapshots were saved with a 1 ps interval.

Because we expect the timescales for oligomer formation to be relatively slow, we employed the following novel approach to facilitate interactions between the peptides. The positions of the peptides were constrained by harmonic coupling [the spring constant, k_c, is 0.02 kcal/(mol Å^2)] between the center of the water box and the oligomer center of mass. The peptide concentration corresponds, within an order of magnitude, to that estimated experimentally for $A\beta_{16-22}$ amyloid deposits. We have checked that the addition of the constraining potential does not alter in any significant way the potential energy of the system. More importantly, the individual peptides are given sufficient volume for efficient conformational sampling in MD simulations. This is reflected in multiple reorientations of individual peptides in $A\beta_{16-22}$ oligomers. A similar, although less general, method of facilitating chain aggregation has been recently used [28].

To establish the general validity of our results, we generated multiple (eight) independent trajectories for both the monomer and the trimer systems. The total simulation time for the monomer system is 64 ns, while the wild-type $(A\beta_{16-22})_3$ oligomer was simulated for 68 ns. For the $(A\beta_{16-22})_3$ oligomer two independent sets of MD simulations were performed, which differ with respect to the initial orientations of the peptides. The centers of mass of the peptides in the initial conformation in the first set of simulations were separated by

about 7 Å. Starting with this conformation and after energy minimization, we obtained four independent heating and equilibration trajectories. Their final conformations served as initial structures for four 10.7 ns production trajectories. These simulations target structural changes that occur upon interpeptide interactions and formation of disordered oligomers.

To probe oligomer ordering on longer timescales, we implemented the following computational strategy. Four independent heating and equilibration trajectories were generated, starting with the initial structure, different from that used in the first set of simulations. Then four preliminary production trajectories were initiated, in which we monitored the population of α and β structures in each peptide. These trajectories were terminated as soon as, in one of them, (1) the average β structure content in two peptides approached 40% and (2) a pair of peptides adopted and maintained approximately antiparallel orientation. The structure satisfying these conditions was used as the starting point for four independent production trajectories of 6.4 ns each.

The rationale for using such a computational strategy is as follows. From the first set of simulations, we observed an accumulation of β strand structures and the formation of salt bridges between peptides. However, the timescale of formation of β strand structures with antiparallel orientation of peptides is too long for direct MD simulations. Thus, we sought to fast-forward the oligomer kinetics by picking up the snapshot with high-β strand content and roughly antiparallel peptide orientation and using it as a starting point for new simulations.

Probes for Amyloid Formation

We used several quantities to characterize structural changes in $A\beta_{16-22}$ oligomers. To characterize the relative orientation of peptides as a function of time, we computed the scalar product of end to end unit vectors, $d_{ij} = \hat{u}_i(t)\hat{u}_j(t)$, for a pair of peptides, i and j. The interpeptide interactions were probed by the distance between the centers of mass of peptides i and j, $R_{ij}^{CM}(t)$, and by the number of interpeptide contacts between side chains, $C_{ij}(t)$. (For the calculation of C_{ij}, side chains are assumed to be in contact if their centers of mass are less than 6.5 Å apart.) We also computed the peptide radii of gyration, $R_{g,i}(t)$. The emergence of stable contacts was evaluated by computing the contact maps as a function of time and the probabilities of formation of individual contacts. The conformational energies of the $(A\beta_{16-22})_3$ oligomer, $E_{pot}^{o}(t)$, and the $A\beta_{16-22}$ monomer, $E_{pot}^{m}(t)$, were monitored as a function of time.

Secondary Structure Probes

Using two definitions of β strand and α helix, we calculated $S_i(H_i)$, the fraction of residues in a peptide, i, whose dihedral angles ϕ and ψ satisfy the definition of local β strand (α helix) structure. Following [29], we assumed ("strict definition") that, for a β strand, $-150^\circ \leq \phi \leq -90^\circ$ and $90^\circ \leq \psi \leq 150^\circ$ and, for an α helix, $-80^\circ \leq \phi \leq -48^\circ$ and $-59^\circ \leq \psi \leq -27^\circ$. The other ("broad") definition [30, 31] assumes that, if ϕ and ψ angles are discretized into 20 intervals of 18°, then β strand conformations correspond to the vertices of the polygon (−180, 180), (−180, 126), (−162, 126), (−162, 108), (−144, 108), (−144, 90), (−50, 90), and (−50, 180) on the Ramachandran plot; the α helix structure is confined to the polygon (−90, 0), (−90, −54), (−72, −54), (−72, −72), (−36, −72), (−36, −18), (−54, −18), and (−54, 0). Both definitions provide qualitatively similar results, although the amount of secondary structure identified with the "strict" definition is predictably smaller. Throughout this study we use the "broad" definition for β strand and α helix. Both ϕ and ψ angles are defined only for five inner residues.

The time dependence of β strand content is obtained with

$$\langle S(t)\rangle = \frac{1}{3M}\sum_{k=1}^{M}\sum_{i=1}^{3} S_i^k(t),$$

where i is the peptide index, k is the trajectory index, and M is the number of trajectories. The average β strand content is computed as $\langle S\rangle = \frac{1}{T}\int_0^T \langle S(t)\rangle dt$, where T is the simulation time. The α helix contents ($\langle H(t)\rangle$ and $\langle H\rangle$), radius of gyration, $\langle R_g(t)\rangle$, and potential energies, $\langle E_{pot}(t)\rangle$, were computed similarly.

To characterize the distribution of $A\beta_{16-22}$ peptide structures, we classify a conformation to be β strand (or α helix) if (1) the (ϕ and ψ) angles of any two consecutive residues are in the corresponding (β strand or α helix) Ramachandran regions and (2) no two consecutive residues are in α helix (β strand) conformations. If neither β strand nor α helix conformations are assigned, then a conformation is classified as RC.

Acknowledgments

We are grateful to Robert Tycko for useful comments. This work was supported in part by a grant from the National Institutes of Health (IR01 NS41356-01). The use of supercomputing resources of the Center for Scientific Computation and Mathematical Modeling at the University of Maryland is gratefully acknowledged.

Received: October 17, 2002
Revised: December 27, 2002
Accepted: January 3, 2003

References

1. Selkoe, D.J. (1999). Translating cell biology into therapeutic advances in Alzheimer's disease. Nature *399*, A23–A31.
2. Hardy, J., and Selkoe, D.J. (2002). The amyloid hypothesis of Alzheimer's disease: progress and problems on the road to therapeutics. Science *297*, 353–356.
3. Lambert, M.P., Barlow, A.K., Chromy, B.A., Edwards, C., Freed, R., Liosatos, M., Morgan, T.E., Rozovsky, I., Trommer, B., Viola, K.L., et al. (1998). Diffusible, nonfibrillar ligands derived from Aβ1–42 are potent central nervous system neurotoxins. Proc. Natl. Acad. Sci. USA *95*, 6448–6453.
4. Walsh, D.M., Hartley, D.M., Kusumoto, Y., Fezoui, Y., Condron, M.M., Lomakin, A., Benedek, G.B., Selkoe, D.J., and Teplow, D.B. (1999). Amyloid β-protein fibrillogenesis. Structure and biological activity of protofibrillar intermediates. J. Biol. Chem. *274*, 25945–25952.
5. Hartley, D.M., Walsh, D.M., Ye, C.P., Diehl, T., Vasquez, S., Vassilev, P.M., Teplow, D.B., and Selkoe, D.J. (1999). Protofibrillar intermediates of amyloid β-protein induce acute electrophysiological changes and progressive neurotoxicity in cortical neurons. J. Neurosci. *19*, 8876–8884.
6. Prusiner, S.B. (1998). Prions. Proc. Natl. Acad. Sci. USA *95*, 13363–13383.
7. Koo, E.H., Lansbury, P.T., Jr., and Kelly, J.W. (1999). Amyloid diseases: abnormal protein aggregation in neurodegeneration. Proc. Natl. Acad. Sci. USA *96*, 9989–9990.
8. Sunde, M., and Blake, C.C.F. (1998). From the globular to the fibrous state: protein structure and structural conversion in amyloid formation. Q. Rev. Biophys. *31*, 1–39.
9. Lynn, D.G., and Meredith, S.C. (2000). Review: model peptides and the physicochemical approach to β-amyloids. J. Struct. Biol. *130*, 153–173.
10. Tycko, R. (2000). Solid-state NMR as a probe of amyloid fibril structure. Curr. Opin. Chem. Biol. *4*, 500–506.
11. Kirkitadze, M.D., Condron, M.M., and Teplow, D.B. (2001). Identification and characterization of key kinetic intermediates in amyloid β-protein fibrillogenesis. J. Mol. Biol. *312*, 1103–1119.
12. Burkoth, T.S., Benzinger, T.L.S., Urban, V., Morgan, D.M., Gregory, D.M., Thiyagarajan, P., Botto, R.E., Meredith, S.C., and Lynn, D.G. (2000). Structure of the β-Amyloid(10–35) fibril. J. Am. Chem. Soc. *122*, 7883–7889.
13. Antzutkin, O.N., Balbach, J.J., Leapman, R.D., Rizzo, N.W., Reed, J., and Tycko, R. (2000). Multiple quantum solid-state NMR indicates a parallel, not antiparallel, organization of β-sheets in Alzheimer's β-amyloid fibrils. Proc. Natl. Acad. Sci. USA *97*, 13045–13050.
14. Lansbury, P.T., Costa, P.R., Griffiths, J.M., Simon, E.J., Auger, M., Halverson, K.J., Kocisko, D.A., Hendsch, Z.S., Ashburn, T.T., Spencer, R.G.S., et al. (1995). Structural model for the beta-amyloid fibril based on interstrand alignment of an antiparallel-sheet comprising a C-terminal peptide. Nat. Struct. Biol. *2*, 990–998.

15. Balbach, J.J., Ishii, Y., Antzutkin, O.N., Leapman, R.D., Rizzo, N.W., Dyda, F., Reed, J., and Tycko, R. (2000). Amyloid fibril formation by $A\beta_{16-22}$, a seven-residue fragment of the Alzheimer's β-amyloid peptide, and structural characterization by solid state NMR. Biochemistry *39*, 13748–13759.
16. Wetzel, R. (2002). Ideas of order for amyloid fibril structure. Structure *10*, 1031–1036.
17. Fersht, A.R., and Daggett, V. (2002). Protein folding and unfolding at atomic resolution. Cell *108*, 573–582.
18. Lee, J.P., Stimson, E.R., Ghilardi, J.R., Mantyh, P.W., Lu, Y.A., Felix, A.M., Llanos, W., Behbin, A., Cummings, M., Van Criekinge, M., et al. (1995). ^{1}H NMR of $A\beta$ amyloid peptide congeners in water solution. Conformational changes correlate with plaque competence. Biochemistry *34*, 5191–5200.
19. Massi, F., Peng, J.W., Lee, J.P., and Straub, J.E. (2001). Simulation study of the structure and dynamics of the Alzheimer's amyloid peptide congener in solution. Biophys. J. *80*, 31–44.
20. Sayle, R., and Milner-White, E.J. (1995). RasMol: biomolecular graphics for all. Trends Biochem. Sci. *20*, 374–376.
21. Chou, P.Y., and Fasman, G.D. (1978). Prediction of the secondary structure of proteins from their amino acid sequence. Adv. Enzymol. *47*, 45–148.
22. Tjernberg, L.O., Callaway, D.J.E., Tjernberg, A., Hahne, S., Lilliehook, C., Terenius, L., Thyberg, J., and Nordstedt, C. (1999). Molecular model of Alzheimer amyloid β-peptide fibril formation. J. Biol. Chem. *274*, 12619–12625.
23. Harper, J.D., and Lansbury, P.T., Jr. (1997). Models of amyloid seeding in Alzheimer's disease and scrapie: mechanistic truths and physiological consequences of time-dependent stability of amyloid proteins. Annu. Rev. Biochem. *66*, 385–407.
24. Griffith, J.S. (1967). Self-replication and scrapie. Nature *215*, 1043–1044.
25. Balbirnie, M., Grothe, R., and Eisenberg, D.S. (2001). An amyloid-forming peptide from the yeast prion Sup35 reveals a dehydrated β-sheet structure for amyloid. Proc. Natl. Acad. Sci. USA *98*, 2375–2380.
26. Elber, R., Roitberg, A., Simmerling, C., Goldstein, R., Li, H., Verkhiver, G., Keasar, C., Zhang, J., and Ulitsky, A. (1994). MOIL: a program for simulation of macromolecules. Comput. Phys. Commun. *91*, 159–189.
27. Darden, T.A., York, D.M., and Pedersen, L.G. (1993). Particle mesh Ewald: an N*log(N) method for Ewald sums in large systems. J. Chem. Phys. *98*, 10089–10092.
28. Dima, R.I., and Thirumalai, D. (2002). Exploring protein aggregation and self-propagation using lattice models: phase diagram and kinetics. Protein Sci. *11*, 1036–1049.
29. Srinivasan, R., and Rose, G.D. (1995). LINUS: a hierarchic procedure to predict the fold of a protein. Proteins Struct. Funct. Genet. *22*, 81–99.
30. Munoz, V., and Serrano, L. (1994). Intrinsic secondary structure propensities of the amino acids, using statistical ϕ-ψ matrices: comparison with experimental scales. Proteins Struct. Funct. Genet. *20*, 301–311.
31. Street, A.G., and Mayo, S.L. (1999). Intrinsic β-sheet propensities result from van der Waals interactions between side chains and the local backbone. Proc. Natl. Acad. Sci. USA *96*, 9074–9076.